VLSI Implementation of a Pipelined 128 points 4-Parallel radix-2³ FFT Architecture via Folding Transformation

James J. W. Kunst `jjwk89@gmail.com`
Kevin H. Viglianco `kevinviglianco@gmail.com`
Daniel R. Garcia `dani6rg@gmail.com`

Digital Signal Processing in Very Large Scale Integration Systems

Autumn 2019

Dr. Keshab K. Parhi
Dr. Ariel L. Pola

Universidad Nacional de Córdoba - FCEFyN
Av.Vélez Sársfield 1611, X5016GCA, Córdoba, Argentina

Fundación FULGOR
Ernesto Romagosa 518, Colinas V. Sarsfield, X5016GQN, Córdoba, Argentina

Abstract—This work describes the design and the VLSI implementation of a 4-parallel pipelined architecture for the complex fast Fourier transform (CFFT) based on the radix-2³ algorithm with 128 points using folding transformation and register minimization techniques. In addition, different synthesis reports from the Hardware Description Language (HDL) using different optimization techniques were studied in order to obtain good performance on speed and area with a clock frequency of $500MHz$ using an open-source FreePDK45 of 45 nm CMOS technology.

Fig. 1: Types of pipelined FFT archicectures for 16 points [2].

I. Introduccion

THE Fast Fourier Transform (FFT) is widely used in different applications fields, particularly in algorithms that involves applying digital signal processing, e.g., calculate the Discrete Fourier Transform (DFT) efficiently. Nowadays is common to use parallel-pipelined architecture in FFT algorithms for real time applications, this allows to achieve good performance with high throughput rates.

There are two main types of pipelined FFT architectures [1]. On one hand, feedback architectures (FB) which can be divided into Single-path Delay Feedback (SDF) and Multi-path Delay Feedback (MDF), both methods transfer data samples between stages serially and use feedback loops. On the other hand, feedforward architectures such as Multi-Path Delay Commutator (MDC) transfers more than one sample per clock cycle and do not use feedback loops.

This work focuses on the design of 4-parallel pipelined architecture *radix*-2³ 128-points for Complex FFT-DIF (Decimation In Frequency). Section II, describes the equations that correspond to Butterfly structure of *radix*-2³ FFT-DIF. In Section III, the design of a 2-parallel pipelined architecture, *radix*-2³ 16-points FFT via folding transformation is presented. In
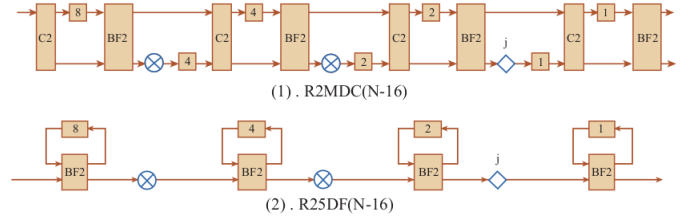
Section IV, the previous design is translate to a 4-parallel, 128-points *radix*-2³ DIF complex FFT, and a float-point simulator in *Matlab* is elaborated, to later be compared with a fixed-point model in order to obtain the best Signal to Quantization Noise Ratio (SQNR). In Section V, different power, area and timing reports with different optimizations such as varying pipelining levels, and the application of canonical signed digit (CSD) are compared to obtain the best performance with a clock frequency of $500MHz$. Finally in Section VI, some conclusions and discussions are presented.

II. Radix-2³ FFT algorithm

The *N*-point DFT of an input sequence $x[n]$ is defined as:

$$X[k] = \sum_{n=0}^{N-1} x[n] \dot{W}_N^{nk}, \quad k = 0, 1, ..., N-1 \tag{1}$$

where $W_N^{nk} = e^{-j\frac{2\pi}{N}nk}$.

Direct computation of the DFT is basically inefficient, primarily because it does not exploit the symmetry and peri-

odicity properties of the phase factor W_N, these two properties are:

$$\text{Symmetry property: } W_N^{k+N/2} = -W_N^k \qquad (2)$$

$$\text{Periodicity property: } W_N^{k+N} = W_N^k \qquad (3)$$

The FFT design based on Cooley-Tukey algorithm is most commonly used to compute the DFT efficiently, this allows to reduce the number of operations from $O(N^2)$ to $O(Nlog_2N)$. The development of computationally efficient algorithms for DFT is possible if a *Divide and Conquer* approach is adopted. This approach is based on the decomposition of an N point DFT into successively smaller DFTs, this means that the DFT is calculated as a series of $s = log_\rho N$ stages, where ρ is the base of the *radix*, e.g., in this work this factor is two, so the number of stages for 128 points is 7.

According to [3], [4], There are two methods to design FFT algorithms:

a) Decimation in time (DIT): In this method the N-point data sequence $x[n]$ is split into two $N/2$-point data sequences, thus, is possible to obtain two different functions by decimating $x[n]$ by a factor of 2. The decimation of the data sequence can be repeated again, until the resulting sequences are reduced to one-point sequence.

b) Decimation in frequency (DIF): This method is based on the divide-and-conquer technique, where the DFT formula is split into two summations, one of which involves the sum over the first $N/2$ data points and the second sum involves the last $N/2$ data points.

In each decomposition, the basic computing unit that processes the samples is called *butterfly*. In general, each butterfly involves one complex multiplication and two complex additions. The main difference between DIT and DIF is the instant in which the multiplication by W_N^ϕ is computed, the input samples can be multiplied before or after the butterfly structure, as is depicted in Fig.2.
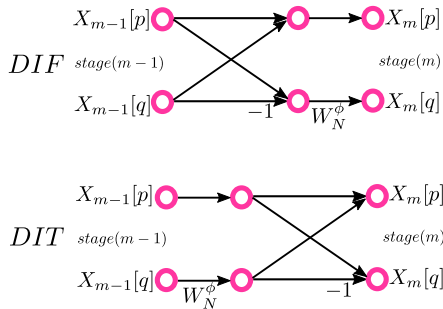

Fig. 2: Basic butterflies computation in the decimation in time and frequency.

Another difference between the two methods is that the input samples in DIF algorithms are organized in natural order but the output are not in order, in which case a reordering circuit at the output is needed, in contrast with the DIT algorithms where the input sequence are not in order but the output is in natural order.

According to the methodology presented in [3], it is possible to apply the mathematical expressions of *radix*-2^3 DIF as is

explain in [5]. These fundamental equations are describe in equation (4):

$$C_{8k+0} = \sum_{n=0}^{N/8-1} \left\{ [(x_n + x_{n+\frac{N}{2}}) + (x_{n+\frac{N}{4}} + x_{n+\frac{3N}{4}})] + \right. \qquad (4)$$
$$\left. [(x_{n+\frac{N}{8}} + x_{n+\frac{5N}{8}}) + (x_{n+\frac{3N}{8}} + x_{n+\frac{7N}{8}})] \right\} W_N^{0n} W_{N/8}^{nk}$$

$$C_{8k+4} = \sum_{n=0}^{N/8-1} \left\{ [(x_n + x_{n+\frac{N}{2}}) + (x_{n+\frac{N}{4}} + x_{n+\frac{3N}{4}})] - \right.$$
$$\left. [(x_{n+\frac{N}{8}} + x_{n+\frac{5N}{8}}) + (x_{n+\frac{3N}{8}} + x_{n+\frac{7N}{8}})] \right\} W_N^{4n} W_{N/8}^{nk}$$

$$C_{8k+2} = \sum_{n=0}^{N/8-1} \left\{ [(x_n + x_{n+\frac{N}{2}}) - (x_{n+\frac{N}{4}} + x_{n+\frac{3N}{4}})] - j \right.$$
$$\left. [(x_{n+\frac{N}{8}} + x_{n+\frac{5N}{8}}) - (x_{n+\frac{3N}{8}} + x_{n+\frac{7N}{8}})] \right\} W_N^{2n} W_{N/8}^{nk}$$

$$C_{8k+6} = \sum_{n=0}^{N/8-1} \left\{ [(x_n + x_{n+\frac{N}{2}}) - (x_{n+\frac{N}{4}} + x_{n+\frac{3N}{4}})] + j \right.$$
$$\left. [(x_{n+\frac{N}{8}} + x_{n+\frac{5N}{8}}) - (x_{n+\frac{3N}{8}} + x_{n+\frac{7N}{8}})] \right\} W_N^{6n} W_{N/8}^{nk}$$

$$C_{8k+1} = \sum_{n=0}^{N/8-1} \left\{ [(x_n - x_{n+\frac{N}{2}}) - j(x_{n+\frac{N}{4}} - x_{n+\frac{3N}{4}})] + W_N^{N/8} \right.$$
$$\left. [(x_{n+\frac{N}{8}} - x_{n+\frac{5N}{8}}) - j(x_{n+\frac{3N}{8}} - x_{n+\frac{7N}{8}})] \right\} W_N^{n} W_{N/8}^{nk}$$

$$C_{8k+5} = \sum_{n=0}^{N/8-1} \left\{ [(x_n - x_{n+\frac{N}{2}}) - j(x_{n+\frac{N}{4}} - x_{n+\frac{3N}{4}})] - W_N^{N/8} \right.$$
$$\left. [(x_{n+\frac{N}{8}} - x_{n+\frac{5N}{8}}) - j(x_{n+\frac{3N}{8}} - x_{n+\frac{7N}{8}})] \right\} W_N^{5n} W_{N/8}^{nk}$$

$$C_{8k+3} = \sum_{n=0}^{N/8-1} \left\{ [(x_n - x_{n+\frac{N}{2}}) + j(x_{n+\frac{N}{4}} - x_{n+\frac{3N}{4}})] + W_N^{3N/8} \right.$$
$$\left. [(x_{n+\frac{N}{8}} - x_{n+\frac{5N}{8}}) + j(x_{n+\frac{3N}{8}} - x_{n+\frac{7N}{8}})] \right\} W_N^{3n} W_{N/8}^{nk}$$

$$C_{8k+7} = \sum_{n=0}^{N/8-1} \left\{ [(x_n - x_{n+\frac{N}{2}}) + j(x_{n+\frac{N}{4}} + x_{n+\frac{3N}{4}})] - W_N^{3N/8} \right.$$
$$\left. [(x_{n+\frac{N}{8}} - x_{n+\frac{5N}{8}}) + j(x_{n+\frac{3N}{8}} - x_{n+\frac{7N}{8}})] \right\} W_N^{7n} W_{N/8}^{nk}$$

Fig. 3 and Fig. 4 show the equivalent diagram of interconnections and data flows from the equations presented in (4).
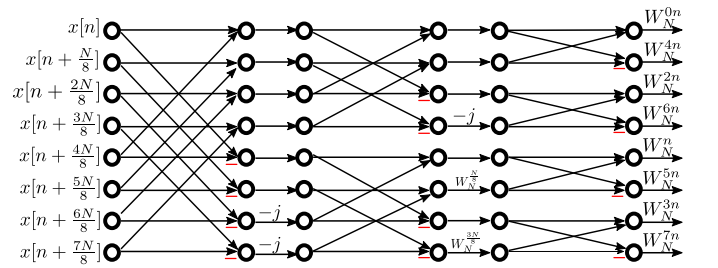

Fig. 3: Structure of interconnection for *radix*-2^3 DIF DFT.

A. 16 points DFT

The next step is to find the suitable rotator factors for the 16 point DFT, the equations in (4) are essential for this design

$$W_N^{\frac{N}{8}} = e^{-j\frac{\pi}{4}} = 0.7071 - j0.7071$$
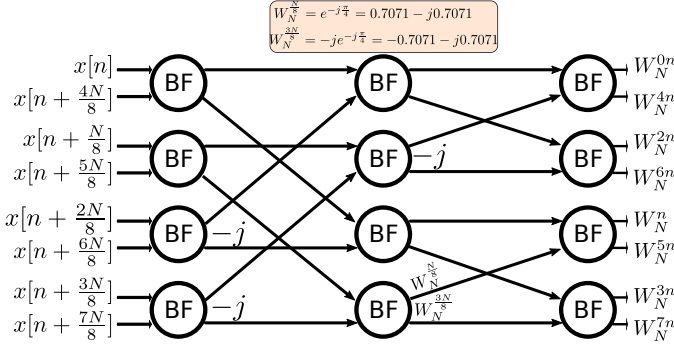$$W_N^{\frac{3N}{8}} = -je^{-j\frac{\pi}{4}} = -0.7071 - j0.7071$$

Fig. 4: Data flow graph (DFG) based in equations (4).

and they were evaluated to get $C_{8k+i} = \sum_{n=0}^{16/8-1}\{\cdot\}$, for $k = 0, 1$. The structure for the 16 point DFT is described in Fig. 5 and Fig. 6.
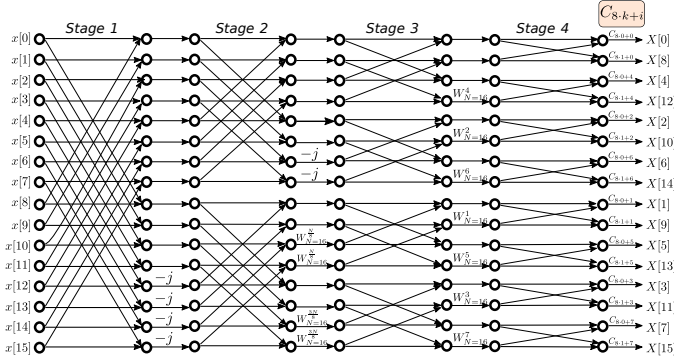
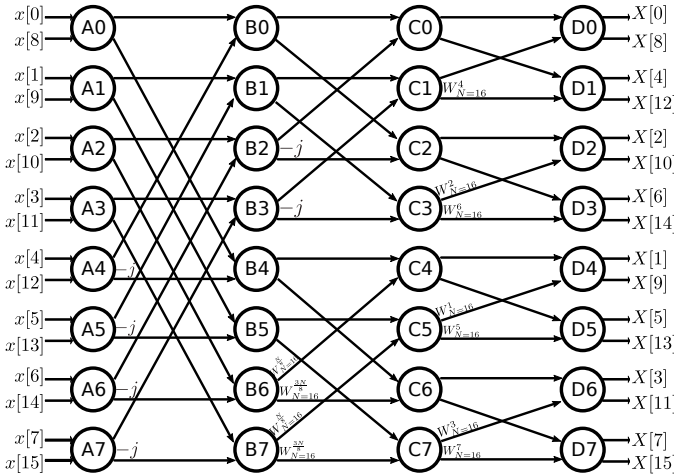Fig. 5: Flow graph of a *radix*-2^3 16-point DIF DFT

Fig. 6: Data flow graph (DFG) for a *radix*-2^3 16-point DIF DFT

B. 128 points DFT

With these first approaches is possible the application of the divide and conquer strategy by decomposing the 128-point DFT and calculating each coefficient $C_{8k+i} = \sum_{n=0}^{128/8-1}\{\cdot\}$, for $k = 0, 1, ..., (128/8) - 1$, this way a chain sequence of butterflies is obtained together with its corresponding rotation factor and the correct index of the samples in which they must

be added or multiplied. Using this technique is possible to do a subdivision of butterflies stages, as is shown in Fig. 7, the decomposition of the 128 point DFT involves three stages of butterflies resulting in a set of eight 16 point DFTs. Finally, Fig. 8 shows the complete architecture for the *radix*-2^3 128-point DIF DFT with a total of seven stages where each stage contains 64 butterflies of radix-2 base.
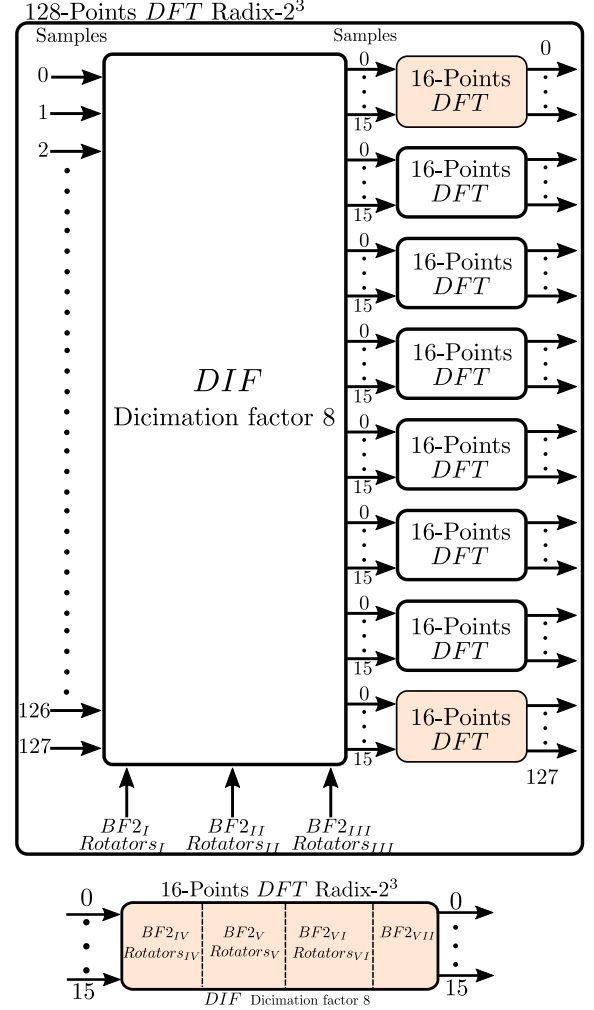
128-Points *DFT* Radix-2^3

16-Points *DFT* Radix-2^3

Fig. 7: Decomposing a *radix*-2^3 128-point DFT.

III. DESIGN OF A FFT ARCHITECTURE VIA FOLDING TRANSFORMATION

In this section, the architecture proposed in [6] together with the folding transformation and register minimization techique described in [7] is used to obtain a 16-point DIF FFT 4-parallel architecture, then, the same method is extended to achieve a 128-point DIF FFT 4-parallel architecture.

A. 4-Parallel radix-2^3 16-Points

The flow graph of a 16-point DIF FFT radix-2^3 with main base radix-2 is shown in Fig. 5. The graph is divided into four stages, each of them consist of a set of butterflies and multipliers. The twiddle factor between the stages indicates a multiplication by W_N^k, where W_N denotes the Nth root of unity,
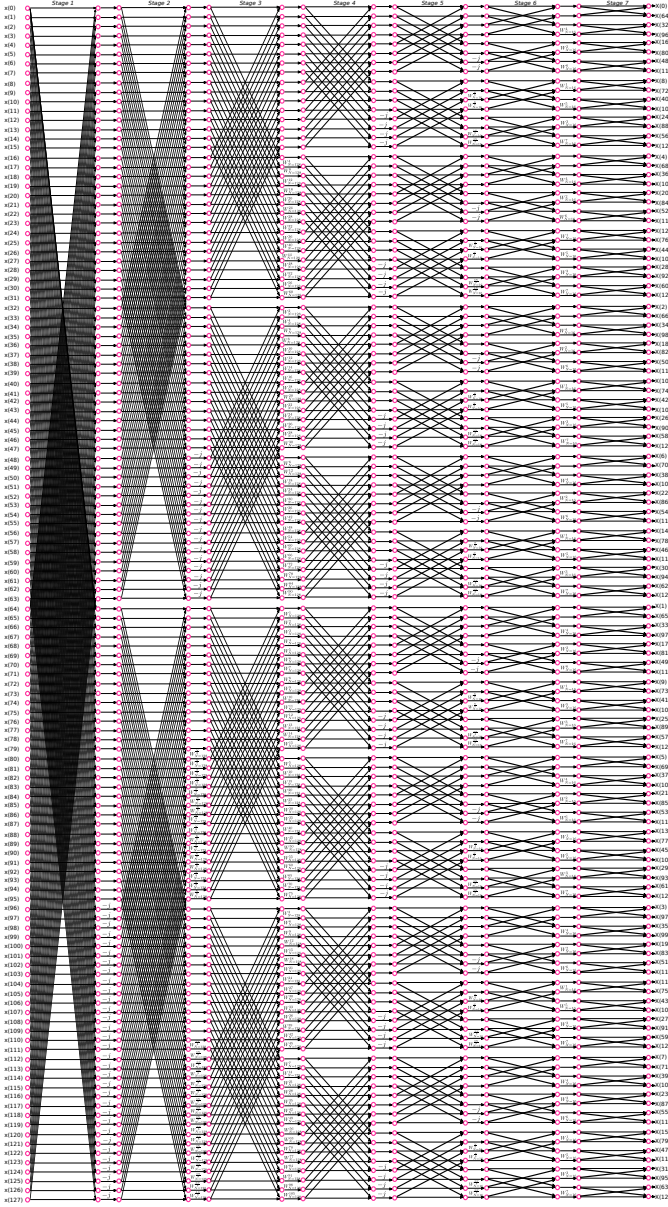
Fig. 8: Flow graph of a *radix*-2^3 128-point DIF DFT

respectively. The folding equation for the edge e is:

$$D_F(U \rightarrow V) = Kw(e) - P_U + v - u \qquad (5)$$

where P_U is the number of pipeline stages in the hardware unit which executes the node U.

Considering the folding of the DFG in Fig. 6 with the folding sets:

$$A = \{A0, A2, A4, A6\} \qquad A' = \{A1, A3, A5, A7\}$$
$$B = \{B1, B3, B0, B2\} \qquad B' = \{B5, B7, B4, B6\}$$
$$C = \{C2, C1, C3, C0\} \qquad C' = \{C6, C5, C7, C4\}$$
$$D = \{D3, D0, D2, D1\} \qquad D' = \{D7, D4, D6, D5\}$$

Assuming that the butterfly operations do not have any pipeline stages ($P_A = P_B = P_C = P_D = 0$), the folding equations can be derived for all edges, thus, the expression *without retiming* can be obtained from (5).

$$D_F(A0 \rightarrow B0) = 2 \qquad D_F(A0 \rightarrow B4) = 2$$
$$D_F(A1 \rightarrow B1) = 0 \qquad D_F(A1 \rightarrow B5) = 0$$
$$D_F(A2 \rightarrow B2) = 2 \qquad D_F(A2 \rightarrow B6) = 2$$
$$D_F(A3 \rightarrow B3) = -1 \qquad D_F(A3 \rightarrow B7) = -1$$
$$D_F(A4 \rightarrow B0) = 0 \qquad D_F(A4 \rightarrow B4) = 0$$
$$D_F(A5 \rightarrow B1) = -1 \qquad D_F(A5 \rightarrow B5) = -1$$
$$D_F(A6 \rightarrow B2) = 0 \qquad D_F(A6 \rightarrow B6) = 0$$
$$D_F(A7 \rightarrow B3) = -2 \qquad D_F(A7 \rightarrow B7) = -2$$
$$D_F(B0 \rightarrow C0) = 1 \qquad D_F(B0 \rightarrow C2) = -2$$
$$D_F(B1 \rightarrow C1) = 1 \qquad D_F(B1 \rightarrow C3) = 2$$
$$D_F(B2 \rightarrow C0) = 0 \qquad D_F(B2 \rightarrow C2) = -3$$
$$D_F(B3 \rightarrow C1) = 0 \qquad D_F(B3 \rightarrow C3) = 1$$
$$D_F(B4 \rightarrow C4) = 1 \qquad D_F(B4 \rightarrow C6) = -2$$
$$D_F(B5 \rightarrow C5) = 1 \qquad D_F(B5 \rightarrow C7) = 2$$
$$D_F(B6 \rightarrow C4) = 0 \qquad D_F(B6 \rightarrow C6) = -3$$
$$D_F(B7 \rightarrow C5) = 0 \qquad D_F(B7 \rightarrow C7) = 1$$
$$D_F(C0 \rightarrow D0) = -2 \qquad D_F(C0 \rightarrow D1) = 0$$
$$D_F(C1 \rightarrow D0) = 0 \qquad D_F(C1 \rightarrow D1) = 2$$
$$D_F(C2 \rightarrow D2) = 2 \qquad D_F(C2 \rightarrow D3) = 0$$
$$D_F(C3 \rightarrow D2) = 0 \qquad D_F(C3 \rightarrow D3) = -2$$
$$D_F(C4 \rightarrow D4) = -2 \qquad D_F(C4 \rightarrow D5) = 0$$
$$D_F(C5 \rightarrow D4) = 0 \qquad D_F(C5 \rightarrow D5) = 2$$
$$D_F(C6 \rightarrow D6) = 2 \qquad D_F(C6 \rightarrow D7) = 0$$
$$D_F(C7 \rightarrow D6) = 0 \qquad D_F(C7 \rightarrow D7) = -2$$

with its exponent evaluated modulo N. This can be represented as a DFG as shown in Fig. 6, where the nodes represents the butterfly computations of the radix-2 FFT algorithm.

The folding transformation is used on the DFG to derive a pipelined architecture, to do this a folding set is needed. A folding set is an ordered set of operations executed by the same functional unit, each folding set contains K entries, where K is called the folding factor. The operation in the *j*th position within the folding set (where goes from 0 to $K-1$) is executed by the functional unit during the time partition, this term is called the folding order. In order to derive the folding equations a node graph is needed, where an edge e is consider to connect the nodes U and V with $w(e)$ delays. Let the executions of the *l*th iteration of the nodes U and V be scheduled at the time units $Kl + u$ and $Kl + v$ respectively, where u and v are the folding orders of the nodes U and V,

For the folded system to be realizable, $D_F(U \rightarrow V) \geq 0$ must hold for all the edges in the DFG. Retiming and/or pipeline can be applied to satisfy this property, if the DFG in Fig. 6 is pipelined/retimmed as shown in Fig. 9 the system is realizable and the folded delays for the edges are given by the equations that represent a folding set *with retiming*.
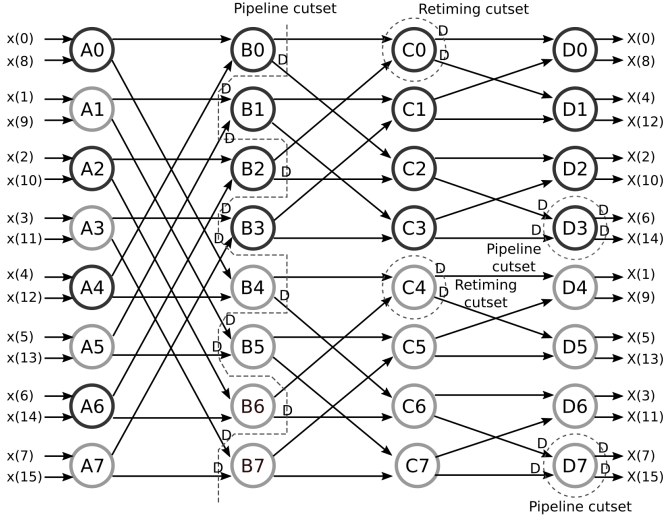
Fig. 9: Data Flow graph (DFG) of a radix-2 16-point DIF FFT with retiming and pipeline.

Fig. 10: Linear lifetime chart for the variables $y_{(0)}, y_{(1)}, ..., y_{(15)}$ for a 16-point FFT architecture.

Fig. 11: Linear lifetime chart for the variables $z_{(0)}, z_{(1)}, ..., z_{(15)}$ for a 16-point FFT architecture.

Fig. 12: Linear lifetime chart for the variables $w_{(0)}, w_{(1)}, ..., w_{(15)}$ for a 16-point FFT architecture.

$$
\begin{aligned}
D_F(A0 \to B0) &= 2 & D_F(A0 \to B4) &= 2 \quad (6)\\
D_F(A1 \to B1) &= 4 & D_F(A1 \to B5) &= 4\\
D_F(A2 \to B2) &= 2 & D_F(A2 \to B6) &= 2\\
D_F(A3 \to B3) &= 3 & D_F(A3 \to B7) &= 3\\
D_F(A4 \to B0) &= 0 & D_F(A4 \to B4) &= 0\\
D_F(A5 \to B1) &= 3 & D_F(A5 \to B5) &= 3\\
D_F(A6 \to B2) &= 0 & D_F(A6 \to B6) &= 0\\
D_F(A7 \to B3) &= 2 & D_F(A7 \to B7) &= 2\\
D_F(B0 \to C0) &= 1 & D_F(B0 \to C2) &= 2\\
D_F(B1 \to C1) &= 1 & D_F(B1 \to C3) &= 2\\
D_F(B2 \to C0) &= 0 & D_F(B2 \to C2) &= 1\\
D_F(B3 \to C1) &= 0 & D_F(B3 \to C3) &= 1\\
D_F(B4 \to C4) &= 1 & D_F(B4 \to C6) &= 2\\
D_F(B5 \to C5) &= 1 & D_F(B5 \to C7) &= 2\\
D_F(B6 \to C4) &= 0 & D_F(B6 \to C6) &= 1\\
D_F(B7 \to C5) &= 0 & D_F(B7 \to C7) &= 1\\
D_F(C0 \to D0) &= 2 & D_F(C0 \to D1) &= 4\\
D_F(C1 \to D0) &= 0 & D_F(C1 \to D1) &= 2\\
D_F(C2 \to D2) &= 2 & D_F(C2 \to D3) &= 4\\
D_F(C3 \to D2) &= 0 & D_F(C3 \to D3) &= 2\\
D_F(C4 \to D4) &= 2 & D_F(C4 \to D5) &= 4\\
D_F(C5 \to D4) &= 0 & D_F(C5 \to D5) &= 2\\
D_F(C6 \to D6) &= 2 & D_F(C6 \to D7) &= 4\\
D_F(C7 \to D6) &= 0 & D_F(C7 \to D7) &= 2
\end{aligned}
$$

The number of registers required to implement the folding equations in (6) is 80, in order to minimize the number of registers the register minimization technique is needed. To apply this technique lets consider the output of node $A0$ to be $y_{(0)}$ and $y_{(8)}$, and the output of the node A1 to be $y_{(1)}$ and $y_{(9)}$, applying this method successively with the rest of the nodes A a linear life time chart for this stage is obtain as is shown in Fig.10. Applying this criteria to the rest of the stages the life time chart for nodes B and C are obtained
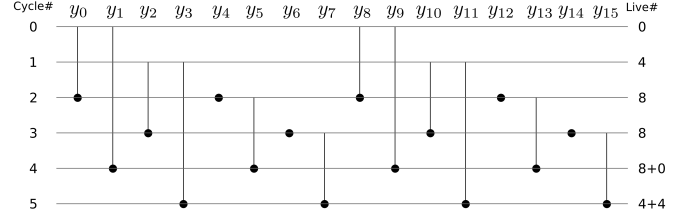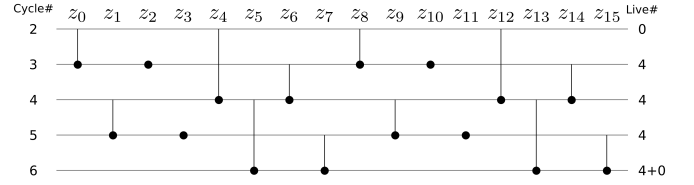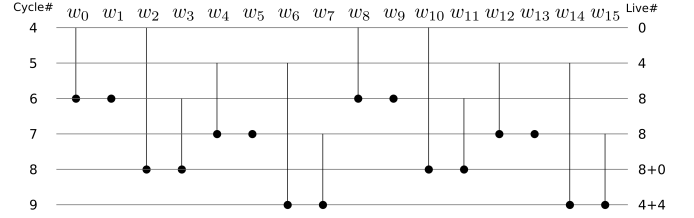
as is shown in Fig.11 and Fig.12 respectively. The resulting maximum number of registers for each stage are 8, 4 and 8 respectively, therefore the total number of registers is reduced from 80 to 20. More information about this method can be found on [7].

The register allocation tables for the lifetime charts are shown in Fig. 13, 14 and 15 for stage A, B and C respectively. Fig.16 and Fig.17 show the designations of registers for the stage A and B respectively used in the allocation tables, the designation for stage C are similar to stage A. The folded architecture in Fig.19 is synthesized using the folding equations and the register allocation tables. The dataflow for each stage can be seen in Tab. I, the control signal for stage A and B can be implemented by dividing the clock signal to 4 and 2 respectively, for stage C the control signal is the same that the stage A. Note that in Fig. 19 the inputs and output are not ordered, to order these variables an extra logic is needed, this imply using more registers and multiplexers.

The inputs for each folding node are represented in a matrix where the values in the same column is the data that flows in parallel, and values in the same row correspond to the data that flows through the same path in consecutive clock cycles. The first two rows represent the inputs of the superior BF and the others two represents the input of the inferior BF. The same criteria is used for represent the rotators constants, where each number k of the matrix represent a multiplication by W_N^k.

#Cycle	Stage 1		Stage 2		Stage 3	
	Dataflow	Control	Dataflow	Control	Dataflow	Control
0	$y0 \to R3$ $y8 \to R7$	0	$z0 \to R2$ $z8 \to R4$	0	$w0 \to R3$ $w8 \to R7$	0
1	$y2 \to R3$ $y10 \to R7$	0	$(z2, z10) \to i/p$ $R1 \to R2,\ R3 \to R4$	1	$w4 \to R3$ $w12 \to R7$	0
2	$(y4, y12, R4) \to i/p$ $R2 \to R3,\ R6 \to R7$	1	$z1 \to R2,\ z9 \to R4$ $R1 \to i/p,\ R3 \to i/p$	0	$(w1, w9, R4) \to i/p$ $R2 \to R3,\ R6 \to R7$	1
3	$(y6, y14, R4) \to i/p$ $R2 \to R3,\ R6 \to R7$	1	$(z3, z11) \to i/p$ $R1 \to R2,\ R3 \to R4$	1	$(w5, s9, R4) \to i/p$ $R2 \to R3,\ R6 \to R7$	1
4	$(R2, R4) \to i/p$	0	$R1 \to i/p,\ R3 \to i/p$	0	$(R2, R4) \to i/p$	0
5	$(R2, R4) \to i/p$	0	$R1 \to R2,\ R3 \to R4$	1	$(R2, R4) \to i/p$	0

TABLE I: Dataflow and mux control for each stage based on registers showed in Fig. 16 and 17.

Fig. 13: Register allocation table for the data represented in 10

Fig. 14: Register allocation table for the data represented in 11

Fig. 15: Register allocation table for the data represented in 12
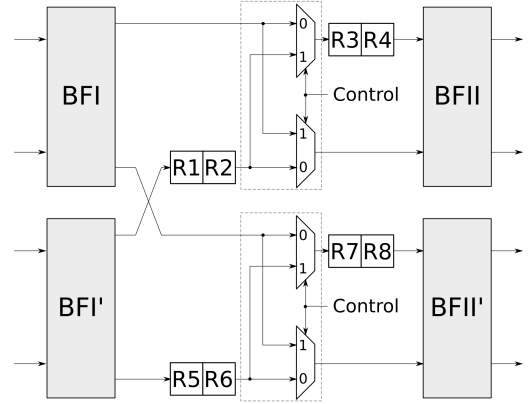
Fig. 16: Registers names used in Fig. 13 for stage 1.
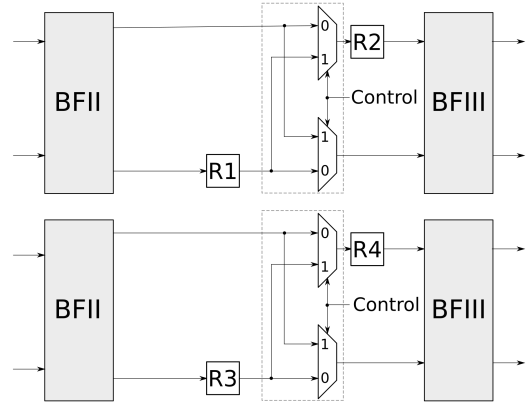
Fig. 17: Registers names used in Fig. 14 for stage 2.

The different types of rotators used in Fig. 19 are shown in Fig. 18, the description of each are:

- Trivial rotator: They can be carried out by interchanging the real and imaginary components and/or changing the sign of the data.
- Constant CSD rotator: They can be carried out by interchanging the real and imaginary components and a multiplication by a unique constant fractional number, in this case we will use a CSD multiplier to reduce the area utilized.
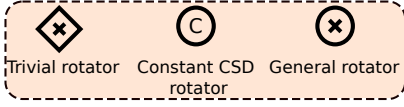
Fig. 18: Symbols used for the different types of rotators

- General rotator: They can be carried out by interchanging the real and imaginary components and/or a multiplication by more than one constant fractional numbers, in this case we will use a general multiplier.

IV. 4-Parallel radix-2^3 128-Points

The previously described method can be used in the design of a 4-Parallel radix-2^3 128-Points architecture. The pipelined/retimmed DFG for this design is shown in Fig. 20, the folding sets are listed in Table II, and in Fig.26 the folded architecture is shown.

A. Implementation of a 128-point FFT

In this section the implementation of the 4-parallel architecture for the computation of 128-point *radix-2^3* DIF complex FFT is described.

In order to compare and validate the operation of the design presented in this work a *MATLAB* simulator has been elaborated to later write a Synthesizable *Verilog* code with different levels of optimizations using a powerful tool like *Synopsys* to get a final design in @45nm Standard Cells [8].

B. Floating and Fixed point Simulator description

The input signal to the design is shown in Fig. 21, the signal will be a mixture of two sinusoid signals with different frequency and normalized amplitude as is describe in equations 7 and 8, where $f_1 = 100Hz$, $f_2 = 1000Hz$ and T_s is the sampled period.

$$x'[n] = cos(2\pi f_1 nT_s) + cos(2\pi f_2 nT_s) \quad (7)$$

$$x[n] = x'[n]/max\{x'[n]\} \quad (8)$$

In each stage of the Fig. 27, input samples that propagate through the stages will be carefully quantized with the purpose of getting a high SQNR (Signal to Quantization Noise Ratio).

$$SQNR_{dB} =$$
$$10log_{10}\left(\frac{Var\{Signal_{FloatPoint}\}}{Var\{Signal_{FloatPoint} - Signal_{FixedPoint}\}}\right) \quad (9)$$

SQNR computation represents the logarithmic relationship between float signal variance over error variance from an given signal.

The input signal $x[n]$ is quantized with a value of $S(10, 9)$, this representation means a signed (S) number with 10 total bits and 9 fractional bits. The value calculated of SQNR for the input is 56.9dB. Following the same steps, we can compute the SQNR for the *twiddle* factors and the design output.

Twiddles factor are quantized with a relation of $S(11, 9)$ and the complex output signal $X[k]$ with $S(22, 15)$, output quantization for the real part is 46.8dB and for the imaginary

part 47.3dB. In general, a value of quantization close to 50dB is a good approximation.

The *MATLAB* fixed-point model is shown in Fig. 27 and Fig.22 shows the output signal in the frequency domain.

The equivalent circuit of the combination of latencies (delays registers) and switches placed between the stages in Fig. 27 are represented in Fig. 23. This circuits are used to appropriately order samples in each butterflies input.

The combination of latencies (delays registers) and switches placed between the stages in Fig. 27 are used to appropriately order samples in each butterflies input and its equivalent circuit is represented in Fig. 23.

The different elements such as multipliers and butterflies process complex numbers as is shown in Fig. 24 and 25, this means that is essential to divide the signal in its real and imaginary part with the purpose of process them independently.

A *general rotator* (full complex multiplier) computes two multiplications and one addition for the real and imaginary part, as is describe in 25, but in case of a *trivial rotator* (multiplication by i), there are no multiplications of additions, it only swap the numbers and change the sign if is necessary, as is shown in Fig .These relations allows to achieve a good design optimization and are important at the moment of calculating the quantization process to ensure an appropriate quantity of bits.

V. Verilog (HDL) Model ,optimizations and results

In this section the different design instances to model the DFT in hardware will be described. With the purpose to have a global view of the optimization levels to achieve the requested *data arrival time* of $1/500Mhz = 2ns$ and the lowest power consumption, four design have been implemented. The design instances were synthesized by Synopsys tool in order to build an interconnection of Standard Cells and generate a complete set of *timing-area-power report* showed in Table III, IV, V and VI.

The first design was made from the base design showed in Fig.26, this hardware model has butterflies modules that work in combination with multipliers and each multiplier has associated a memory block that contains the twiddle factors. In this first approach all multipliers are *full*, each stage has a control module that enables the inversion of the switching block, this control signal is also sent to the multipliers in order to work synchronously with the switching. To avoid the bit growth generated by the addition and multiplication, a quantization block is necessary, the quantizer consist of saturation and truncate operations. The synthesis report is summarize in Table III, notice that a total power consumption is 695.564mW and the data arrival time is greater than minimum period established of 2ns resulting in a time violation. In order to minimize the *critical path* and consumption a second design with *pipelined* registers after the quantization blocks was implemented, and also the *trivial* multipliers (multiplication by $-1j$) were implemented in stages one, two and four, this significantly reduced the size of the binary word resulting in a reduction in the total power as is shown in Table IV, however
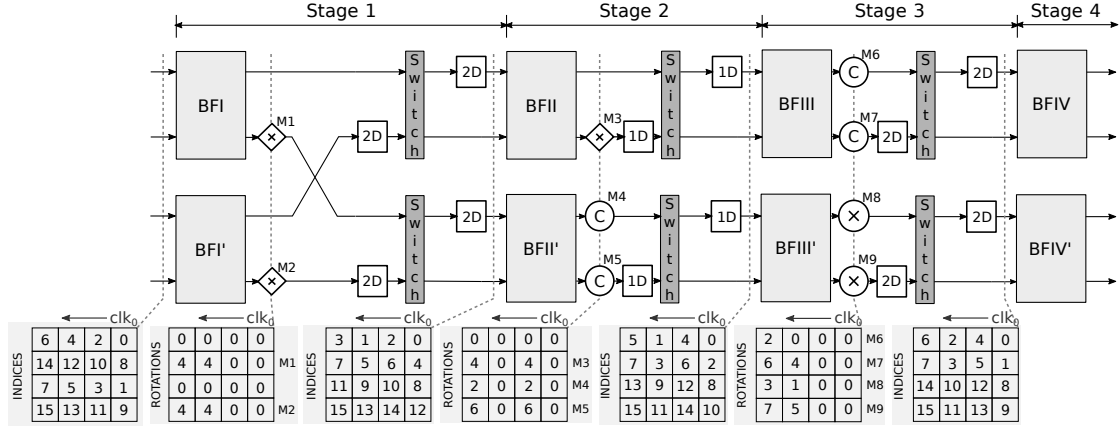
Fig. 19: Folding architecture for the computation of a radix-2^3 16-point DIF complex FFT.

TABLE II: Folding set for the DFG showed in Fig. 20.

A	A0	A2	A4	A6	A8	A10	A12	A14	A16	A18	A20	A22	A24	A26	A28	A30
	A32	A34	A36	A38	A40	A42	A44	A46	A48	A50	A52	A54	A56	A58	A60	A62
A'	A1	A3	A5	A7	A9	A11	A13	A15	A17	A19	A21	A23	A25	A27	A29	A31
	A33	A35	A37	A39	A41	A43	A45	A47	A49	A51	A53	A55	A57	A59	A61	A63
B	B1	B3	B5	B7	B9	B11	B13	B15	B17	B19	B21	B23	B25	B27	B29	B31
	B0	B2	B4	B6	B8	B10	B12	B14	B16	B18	B20	B22	B24	B26	B28	B30
B'	B33	B35	B37	B39	B41	B43	B45	B47	B49	B51	B53	B55	B57	B59	B61	B63
	B32	B34	B36	B38	B40	B42	B44	B46	B48	B50	B52	B54	B56	B58	B60	B62
C	C16	C18	C20	C22	C24	C26	C28	C30	C1	C3	C5	C7	C9	C11	C13	C15
	C17	C19	C21	C23	C25	C27	C29	C31	C0	C2	C4	C6	C8	C10	C12	C14
C'	C48	C50	C52	C54	C56	C58	C60	C62	C33	C35	C37	C39	C41	C43	C45	C47
	C49	C51	C53	C55	C57	C59	C61	C63	C32	C34	C36	C38	C40	C42	C44	C46
D	D8	D10	D12	D14	D16	D18	D20	D22	D24	D26	D28	D30	D1	D3	D5	D7
	D9	D11	D13	D15	D17	D19	D21	D23	D25	D27	D29	D31	D0	D2	D4	D6
D'	D40	D42	D44	D46	D48	D50	D52	D54	D56	D58	D60	D62	D33	D35	D37	D39
	D41	D43	D45	D47	D49	D51	D53	D55	D57	D59	D61	D63	D32	D34	D36	D38
E	E4	E6	E8	E10	E12	E14	E16	E18	E20	E22	E24	E26	E28	E30	E1	E3
	E5	E7	E9	E11	E13	E15	E17	E19	E21	E23	E25	E27	E29	E31	E0	E2
E'	E36	E38	E40	E42	E44	E46	E48	E50	E52	E54	E56	E58	E60	E62	E33	E35
	E37	E39	E41	E43	E45	E47	E49	E51	E53	E55	E57	E59	E61	E63	E32	E34
F	F2	F4	F6	F8	F10	F12	F14	F16	F18	F20	F22	F24	F26	F28	F30	F1
	F3	F5	F7	F9	F11	F13	F15	F17	F19	F21	F23	F25	F27	F29	F31	F0
F'	F34	F36	F38	F40	F42	F44	F46	F48	F50	F52	F54	F56	F58	F60	F62	F33
	F35	F37	F39	F41	F43	F45	F47	F49	F51	F53	F55	F57	F59	F61	F63	F32
G	G3	G5	G7	G9	G11	G13	G15	G17	G19	G21	G23	G25	G27	G29	G31	G0
	G2	G4	G6	G8	G10	G12	G14	G16	G18	G20	G22	G24	G26	G28	G30	G1
G'	G35	G37	G39	G41	G43	G45	G47	G49	G51	G53	G55	G57	G59	G61	G63	G32
	G34	G36	G38	G40	G42	G44	G46	G48	G50	G52	G54	G56	G58	G60	G62	G33

the time violation was still detected in this design. In the third case of optimization an internal pipelined to each butterfly block was added in order to reduce the critical path even more, as the results shown in Table V, this design achieves the data required time. Finally, in the fourth level of optimization showed in Fig.27, the full multipliers from stage two and five were modified to work with *CSD*, achieving a total power consumption of 646.924mW.

VI. CONCLUSIONS

This work has presented a VLSI Implementation of a Pipelined 128 points 4-Parallel radix-2^3 FFT architecture via folding transformation. The folding transformation applied reduced significantly (equal to the folded factor, i.e. 64 times) the number of functional units, and therefore the silicon area at the expense of increasing the computation time by the same factor. Folding technique resulted in an architecture that uses a large number of registers, however by applying a register minimization technique the number of register were significantly reduced from .... to 188 resulting in a final design with less area and power consumption. As for the fixed point implementation, a high SQNR of 46.8dB and 47.3dB for the real and the imaginary part respectably was able to achieve by using saturation and truncation blocks. Lastly a series of optimization were necessary to accomplish the required working frequency. The DFT implementation without any optimization level got to work at 166MHz. Applying a series of pipelines cutsets in the quantization and butterflies blocks the final architecture is implementable at the required clock frequency (500 MHz) at the cost of incrementing the numbers of sequential cells. Finally, by using CSD multipliers a significantly reduction in combinational cells was possible resulting in a even more reduction in the total power consumption. The implementations evolution is summarize in a bar chart in
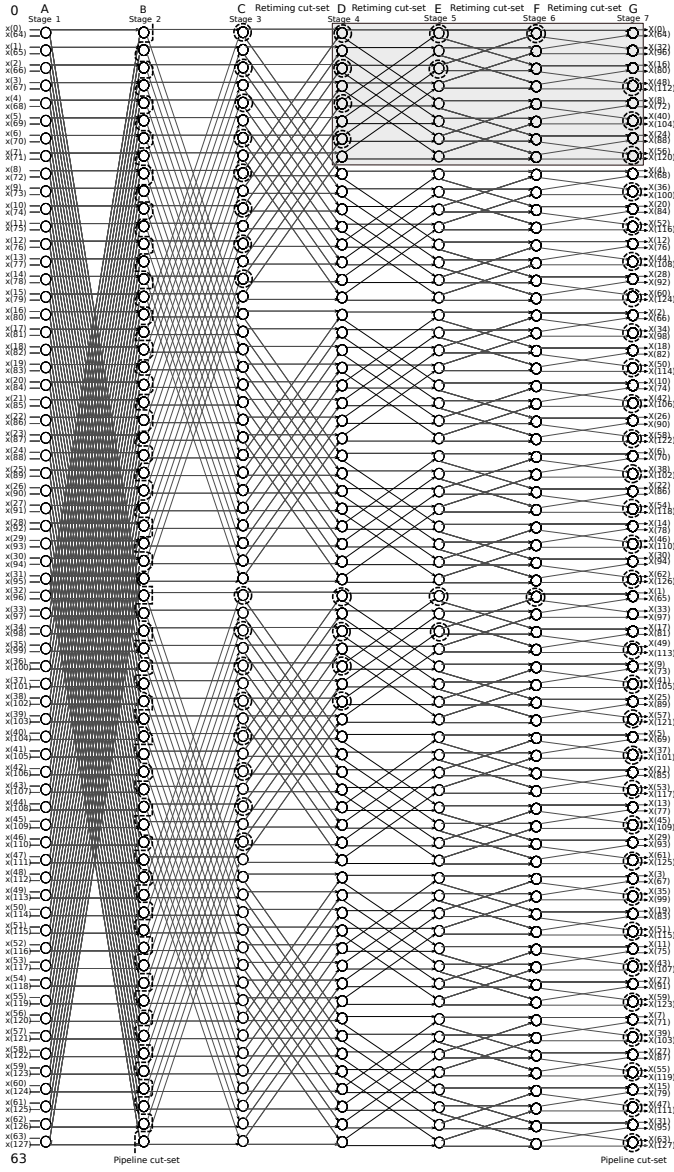
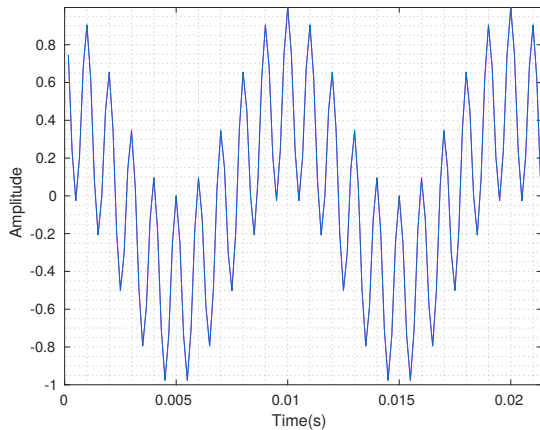Fig. 20: Pipelined/retimmed DFG of a radix-2^3 128-point DIF complex FFT.
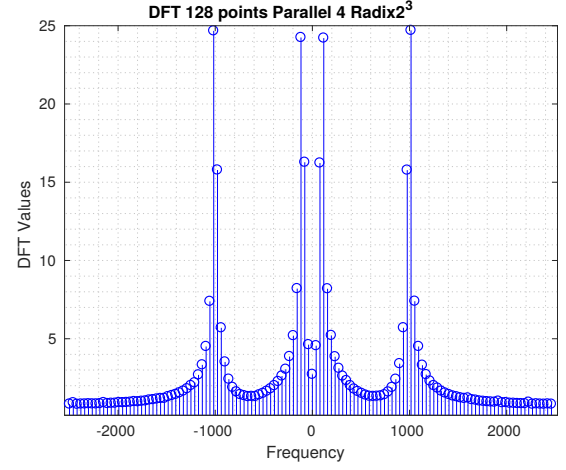

Fig. 22: Output samples, absolute value vs frequency $|X[k]|$
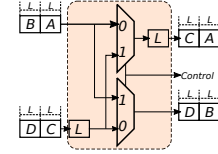

Fig. 23: Circuit for data shuffling
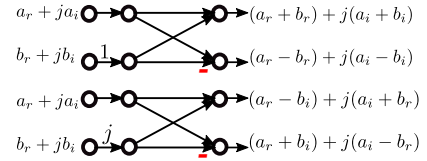
Fig. 24: Complex butterfly
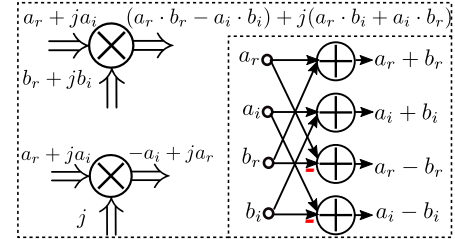
Fig. 25: Complex multiplier and complex adder

Fig. 28, where the last implementation (Imp 4) achieves the require critical path to address the requested *data arrival time* (Slack equals to 0 ns), and also the lowest area and power consumption is obtain. As a final commentary, is worth to notice that in order to use this implementation in a real time application a reordering circuit at the input and the output of the system needs to be include, this circuit present an additional area and power consumption to be considered in the final design.

Fig. 21: Input signal $x[n]$ in time domain

Fig. 26: Folding architecture for the computation of a radix-2^3 128-point DIF complex FFT.

Fig. 27: Quantization for a 128-point 4-parallel complex FFT architecture

Fig. 28: Timing-Area-Power evolution.

TABLE III: Design instance 1. Timing-Area-Power Report at 500MHz.

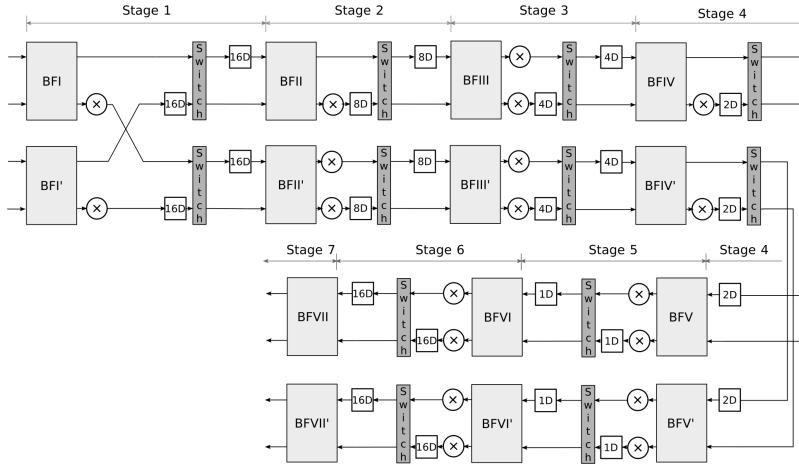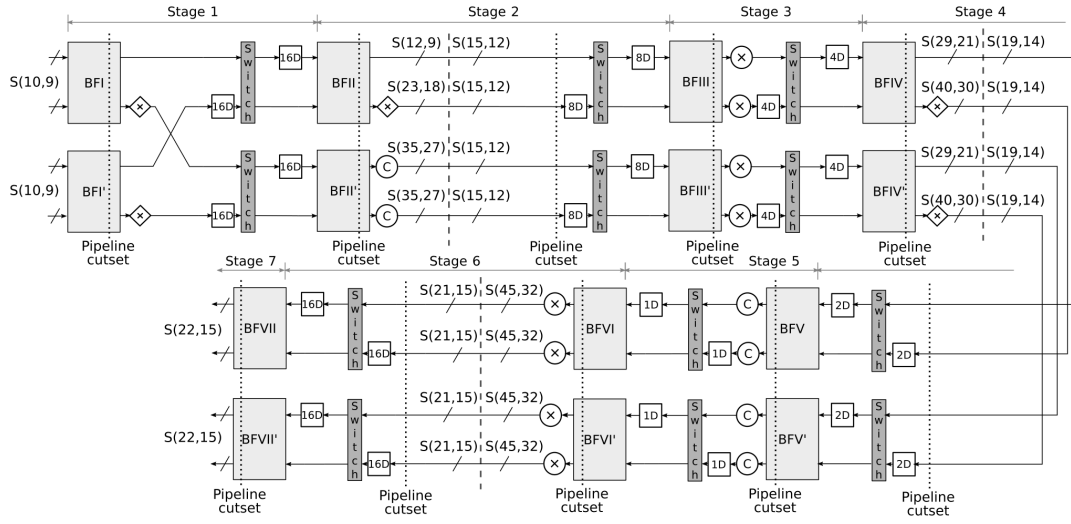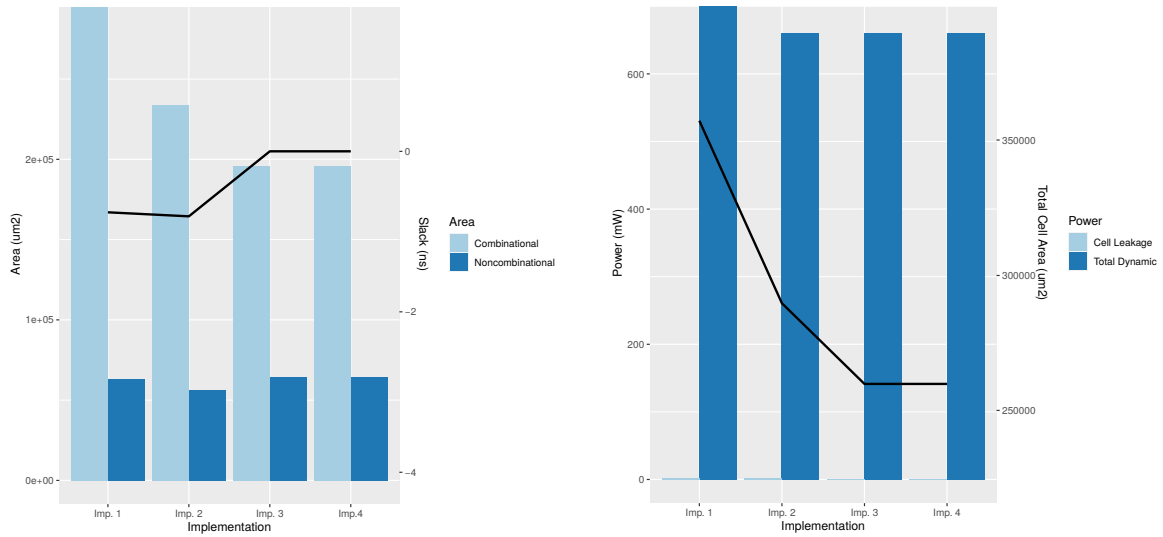| Point	Path(ns)
data arrival time	5.60
clock CLK (rise edge)	2.00
clock network delay (ideal)	2.00
library setup time	1.95
data required time	1.95
data arrival time	-5.60
slack (VIOLATED)	-3.65

Logical Elements	
Number of ports	1228
Number of nets	112376
Number of cells	102726
Number of combinational cells	95310
Number of sequential cells	7404
Number of macros/black boxes	0
Number of buf/inv	27817
Combinational area	291201.116637
Buf/Inv area	44892.767764
Noncombinational area	58830.508095
Total cell area	350031.624731

Power Group	Internal	Switching	Leakage	Total Power
io pad	0.0000	0.0000	0.0000	0.0000
clock network	34.8220	603.2268	1.4573e+06	639.6328
register	54.2228	0.2699	4.0540e+05	54.8980
sequential	0.0000	0.0000	0.0000	0.0000
combinational	0.2884	0.7304	1.5016e+04	1.0337
Total	89.333mW	604.227mW	1.877e+06nW	695.564mW

TABLE IV: Design instance 3. Timing-Area-Power Report at 500MHz.

Point	Path(ns)
data arrival time	2.76
clock CLK (rise edge)	2.00
clock network delay (ideal)	2.00
library setup time	1.95
data required time	1.95
data arrival time	-2.76
slack (VIOLATED)	-0.81

Logical Elements	
Number of ports	1571
Number of nets	94523
Number of cells	87311
Number of combinational cells	80220
Number of sequential cells	7076
Number of macros/black boxes	0
Number of buf/inv	23823
Combinational area	233949.801414
Buf/Inv area	36323.350042
Noncombinational area	56229.647552
Total cell area	290179.448967

Power Group	Internal	Switching	Leakage	Total Power
io pad	0.0000	0.0000	0.0000	0.0000
clock network	24.2875	583.5885	1.0269e+06	608.9492
register	51.0349	0.1728	3.8748e+05	51.5952
sequential	0.0000	0.0000	0.0000	0.0000
combinational	0.9554	1.1271	1.8640e+05	2.2689
Total	76.277mW	584.888mW	1.600e+06nW	662.813mW

TABLE V: Design instance 4. Timing-Area-Power Report at 500MHz.

Point	Path(ns)
data arrival time	1.94
clock CLK (rise edge)	2.00
clock network delay (ideal)	2.00
library setup time	1.94
data required time	1.94
data arrival time	-1.94
slack (MET)	0.00

Logical Elements	
Number of ports	2315
Number of nets	75713
Number of cells	66284
Number of combinational cells	58017
Number of sequential cells	8240
Number of macros/black boxes	0
Number of buf/inv	14789
Combinational area	195877.841872
Buf/Inv area	24429.880240
Noncombinational area	64463.046570
Total cell area	260340.888442

Power Group	Internal	Switching	Leakage	Total Power
io pad	0.0000	0.0000	0.0000	0.0000
clock network	18.1655	581.6307	7.8320e+05	600.6672
register	58.2275	0.2873	4.4422e+05	58.9591
sequential	0.0000	0.0000	0.0000	0.0000
combinational	0.7768	0.9958	1.5970e+05	1.9322
Total	77.169mW	582.913mW	1.387e+06nW	661.558mW

TABLE VI: Design instance 5. Timing-Area-Power Report at 500MHz.

Point	Path(ns)
data arrival time	1.94
clock CLK (rise edge)	2.00
clock network delay (ideal)	2.00
library setup time	1.94
data required time	1.94
data arrival time	-1.94
slack (MET)	0,00

Logical Elements	
Number of ports	2192
Number of nets	55840
Number of cells	48628
Number of combinational cells	40551
Number of sequential cells	8054
Number of macros/black boxes	0
Number of buf/inv	9158
Combinational area	134844.907554
Buf/Inv area	14112.789311
Noncombinational area	64112.010178
Total cell area	198956.917732

Power Group	Internal	Switching	Leakage	Total Power
io pad	0.0000	0.0000	0.0000	0.0000
clock network	19.9015	560.4803	4.9715e+05	580.8741
register	61.1289	1.4388	4.4180e+05	63.0096
sequential	0.0000	0.0000	0.0000	0.0000
combinational	1.5451	1.3368	1.5871e+05	3.0405
Total	82.575mW	563.255mW	1.097e+06nW	646.924mW

REFERENCES

[1] Shousheng He and M. Torkelson, "Designing pipeline FFT processor for OFDM (de)modulation," in *1998 URSI International Symposium on Signals, Systems, and Electronics. Conference Proceedings (Cat. No.98EX167)*. IEEE, pp. 257–262.

[2] V. Stojanovic, "Fast Fourier Transform:VLSI Architectures," *6.973 Communication System Design – Spring 2006 Massachusetts Institute of Technology*, pp. 3–4, 2006.

[3] J. G. Proakis and D. G. Manolakis, "DIGITAL SIGNAL PROCESSING," p. 1033.

[4] A. V. Oppenheim and R. W. Schafer, *Tratamiento de señales en tiempo discreto, tercera edición*. Pearson Educación, OCLC: 843859190.

[5] L. Jia, Y. Gao, and H. Tenhunen, "Efficient VLSI implementation of radix-8 FFT algorithm," p. 4.

[6] M. Ayinala, M. Brown, and K. K. Parhi, "Pipelined Parallel FFT Architectures via Folding Transformation," *IEEE Transactions on Very Large Scale Integration (VLSI) Systems*, vol. 20, no. 6, pp. 1068–1081, Jun. 2012.

[7] K. K. Parhi, *VLSI Digital Signal Processing Systems. Design and implementation*. JOHN WILEY & SONS, INC., 1999, ch. Folding Transformation, pp. 151–163.

[8] R. Thapa, S. Ataei, and J. E. Stine, "WIP. Open-source standard cell characterization process flow on 45 nm (FreePDK45), 0.18 µm, 0.25 µm, 0.35 µm and 0.5 µm," in *2017 IEEE International Conference on Microelectronic Systems Education (MSE)*. Lake Louise, AB, Canada: IEEE, May 2017, pp. 5–6.